

Structural transition and uranium valence change in UTe_2 at high pressure revealed by x-ray diffraction and spectroscopy

Yuhang Deng^{1,*}, Eric Lee-Wong^{1,*}, Camilla M. Moir,¹ Ravhi S. Kumar,² Nathan Swedan¹,
Changyong Park³, Dmitry Yu Popov³, Yuming Xiao³, Paul Chow,³ Ryan E. Baumbach^{4,5}, Russell J. Hemley⁶,
Peter S. Riseborough,⁷ and M. Brian Maple^{1,†}

¹*Department of Physics, University of California, San Diego, California 92093, USA*

²*Department of Physics, University of Illinois Chicago, Chicago, Illinois 60607, USA*

³*High Pressure Collaborative Access Team, X-ray Science Division, Argonne National Laboratory, Argonne, Illinois 60439, USA*

⁴*National High Magnetic Field Laboratory, Florida State University, Tallahassee, Florida 32306, USA*

⁵*Department of Physics, Florida State University, Tallahassee, Florida 32306, USA*

⁶*Departments of Physics, Chemistry, and Earth and Environmental Sciences, University of Illinois Chicago, Chicago, Illinois 60607, USA*

⁷*Department of Physics, Temple University, Philadelphia, Pennsylvania 19122, USA*



(Received 13 March 2024; revised 1 August 2024; accepted 6 August 2024; published 21 August 2024)

High-pressure x-ray diffraction up to 30 GPa, in conjunction with resonant emission x-ray spectroscopy and partial fluorescence yield x-ray absorption spectroscopy up to 52 GPa, were used to study how the structural and electronic properties of UTe_2 evolve with pressure at room temperature. An orthorhombic-to-tetragonal phase transition was observed to occur between 5 and 7 GPa, with a large volume collapse of nearly 10% and a nearest U-U distance increase by about 4%. This lower-to-higher symmetry transition suggests less $5f$ electron participation in bonding when the weakly correlated superconducting phase in the tetragonal structure of UTe_2 appears. Beyond 7 GPa, no new structural transitions were found up to 30 GPa. The resonant x-ray emission spectra clearly demonstrate an intermediate valence of U, nearly $+3.74$ at 1.8 GPa and room temperature, and reveal that the U valence shifts towards $4+$, passes through a peak at 2.8 GPa, then decreases towards $3+$ and settles down to a nearly constant value above 15 GPa. These experiments reveal that some fundamental structural and valence changes occur in UTe_2 at relatively low pressures, which could be responsible for the interplay between unconventional superconductivity, magnetic ordering, and weakly correlated superconductivity that is manifested in the temperature-pressure phase diagram of UTe_2 .

DOI: [10.1103/PhysRevB.110.075140](https://doi.org/10.1103/PhysRevB.110.075140)

I. INTRODUCTION

The heavy-fermion f -electron superconductor UTe_2 has attracted a great deal of attention, driven by an interest in developing a fundamental understanding of its extraordinary unconventional superconducting properties and the possibility that it exhibits spin-triplet superconductivity with potential applications in quantum computation [1,2]. The compound UTe_2 has an enormous reentrant upper critical field $H_{c2}(T)$ of the order of 40 T, considering its low superconducting critical temperature T_c of only 2 K. In addition, there is a pocket of high magnetic field superconductivity (so-called Lazarus phase) which occurs at magnetic fields B between 40 and 60 T and at angles θ between 23° and 45° , where θ is measured with respect to the b axis in the $b-c$ plane of the UTe_2 body-centered orthorhombic unit cell [3,4].

Our approach to study the electronic properties of UTe_2 uses pressure (P) to tune electronic interactions in UTe_2 . Pressure (P) is a clean and powerful parameter for tuning electronic interactions in heavy-fermion compounds, often

resulting in dramatic changes in physical properties in the vicinity of a critical pressure P_c at which a second-order phase transition, usually antiferromagnetic, has been suppressed to 0 K, referred to as a quantum critical point (QCP). Remarkably, unconventional forms of superconductivity, exotic magnetic phases, and non-Fermi-liquid behavior are often found in the vicinity of the QCP. For UTe_2 , specific-heat and electrical transport measurements reveal that pressure suppresses the superconducting transition temperature and induces an antiferromagnetic QCP with non-Fermi-liquid character [5]. We applied two different spectroscopic techniques, U L_3 -edge partial fluorescence yield x-ray absorption spectroscopy (PFY-XAS) and resonant x-ray emission spectroscopy (RXES), to explore the U valence change and the degree of $5f$ electron delocalization in UTe_2 under high pressure. The U L_3 edge was chosen because of the better energy resolution from the longer $3d$ core-hole lifetime (~ 4 eV) compared to the $2p$ core-hole lifetime (~ 8 eV) [6]. The $L_{\alpha 1}$ emission from the $3d$ to $2p$ transition was found to split due to different screening effects on the $2p$ core hole by the $5f$ electron in different configurations [7,8], pointing unambiguously to the multiconfigurational features of U in UTe_2 . X-ray diffraction (XRD) measurements under high P were also used to determine the P dependence of the lattice parameters a , b ,

*These authors contributed equally to this work.

†Contact author: mbmaple@ucsd.edu

and c , and volume of the body-centered orthorhombic unit cell of UTe_2 , and search for possible crystallographic phase transitions. Measurements were taken at room temperature (RT) up to 30 GPa for XRD and up to 52 GPa for PFY-XAS and RXES.

From XRD data, we observed a structural phase transition from the body-centered orthorhombic structure (space group $Immm$) to the body-centered tetragonal structure (space group $I4/mmm$) in the range of 5–7 GPa, confirming the results in Refs. [9,10] at ~ 5 and ~ 4 GPa, respectively. A non-monotonic change in the $U L_3$ white-line position was seen in the PFY-XAS spectra, which indicates a pressure-induced change in the U valence or a change in the degree of localization of the $5f$ electrons. From RXES measurements, we found evidence for an initial increase in the U valence toward $4+$ up to 2.8 GPa, in partial agreement with the x-ray absorption near edge structure (XANES) measurements in Ref. [5] and the XANES and x-ray magnetic circular dichroism measurements in Ref. [11]. Strikingly, with increasing pressure beyond 2.8 GPa, the U valence drops toward $3+$ until ~ 15 GPa, where it remains stable up to 52 GPa. The unusual U valence change and the appearance of the high-pressure tetragonal phase harboring another superconducting state [10] may be related and warrants further investigation.

II. EXPERIMENTAL METHODS

UTe_2 single crystals were grown by chemical vapor transport and then powdered for the measurements. Two batches of samples (S1 and S2) were measured in this work. Batch S1 was grown following the method described in Ref. [12]. Batch S2 was synthesized using the following procedure: uranium and tellurium in a 2:3 atomic ratio were sealed in a quartz tube with 3 mg/cm³ of iodine and kept at a temperature gradient of 1060° C at the hot end and 1000° C at the cold end for 2 weeks. Two high-pressure XRD runs on S1 and S2 were carried out at RT in beamline 16-BMD of HPCAT, the Advanced Photon Source (APS) in Debye-Scherrer geometry. Uranium L_3 -edge RXES and PFY-XAS data at RT under various pressures were collected using samples from batch S1 at the HPCAT 16-IDB beamline. Fluorinert FC70 : FC77 = 1:1 was used as the pressure-transmitting medium for these high-pressure measurements. More details are in Supplemental Material [13].

III. RESULTS AND DISCUSSION

A. High-pressure XRD

Figure 1 shows waterfall plots of the UTe_2 (S1 and S2) XRD spectra under high pressure up to 30 and 20 GPa, respectively. At near-ambient pressure, the UTe_2 XRD spectra were identified with an orthorhombic structure and space group $Immm$ [14] with no impurities. Obvious changes in the diffraction patterns, seen in Fig. 1(b), between 5 and 7 GPa, indicate that a structural phase transition has occurred. The transition is complete at ~ 8 GPa, which agrees with results of Refs. [9,10], with no further phase transitions observed up to 30 GPa. Small discrepancies in the transition pressure could be explained by our choice of different pressure-transmitting media.

The reduced number of peaks in the XRD spectra of the high-pressure phase indicates an increased symmetry, which was identified as a body-centered tetragonal structure (space group $I4/mmm$) [9,10,15]. Following the analyses in Refs. [9,10,15], the lattice parameters (a , b , c) and unit-cell volume (V) of UTe_2 under pressure were calculated via Rietveld refinement of XRD peaks using the open-source software GSAS-II [16], and are shown in Fig. 2. The atomic positions of U and Te atoms in the unit cell of the orthorhombic–tetragonal phase were also refined and used to find the pressure dependence of the nearest uranium-to-uranium distance, d_{U-U} , in Fig. 3. The initial unit-cell volume (V_0) was refined from ambient-pressure XRD spectra taken at RT from the same batch used in subsequent high-pressure XRD measurements. Structural data (i.e., transition pressure, lattice parameters, d_{U-U}) derived from measurements on the two batches S1 and S2 of UTe_2 are in good agreement.

By fitting V/V_0 vs P data, we were able to extrapolate the equations of state for the orthorhombic and tetragonal phases to 7 GPa (midpoint of the structural phase transition) and found that both samples of UTe_2 exhibit a relative volume decrease $\Delta V/V_0 \approx 10\%$ at the phase transition [Fig. 2(d)]. The b axis of the low-pressure orthorhombic lattice has the largest compression of $\sim 33\%$ at the phase transition, followed by $\sim 27\%$ for the c axis and $\sim 3\%$ for the a axis. The bulk modulus (K_0) and differential bulk modulus (dK_0/dP) were calculated by fitting a third-order Birch-Murnaghan equation of state [9] to the V vs P data,

$$P(V) = \frac{3}{2}K_0 \left[\left(\frac{V_0}{V} \right)^{7/3} - \left(\frac{V_0}{V} \right)^{5/3} \right] \times \left\{ 1 + \frac{3}{4} \left(\frac{dK_0}{dP} - 4 \right) \left[\left(\frac{V_0}{V} \right)^{2/3} - 1 \right] \right\}. \quad (1)$$

In Table I, we list the fitting parameters of the third-order Birch-Murnaghan equation of state for our data shown in Fig. 2(d).

The value of K_0 (average ~ 59 GPa) for the orthorhombic phase is comparable to those reported in Ref. [9] (~ 44 GPa) and Ref. [10] (~ 59 GPa). The high-pressure tetragonal UTe_2 phase has a stiffer bulk modulus of ~ 65 GPa, which is smaller than the value (~ 74 GPa) obtained in Ref. [9]. The bulk modulus of the orthorhombic phase is small, comparable to tellurium (65 GPa), suggesting UTe_2 is a very soft material whose physical properties are more responsive to changes in pressure. Interestingly, tellurium also undergoes a hexagonal-to-monoclinic structural transition at about 4 GPa [17], which is similar to the onset pressure for the structural phase transition for UTe_2 . The change in d_{U-U} with pressure was also calculated for the two structures and is shown in Fig. 3. Notably, d_{U-U} increased at the structural phase transition from ~ 3.7 to ~ 3.9 Å, comparable to the values reported in Refs. [9,10]. Even at 30 GPa, d_{U-U} is still above the Hill limit for uranium compounds (3.4–3.6 Å).

Using the CALYPSO software package and Vienna *Ab initio* Simulation package (VASP), Hu *et al.* predicted that the $Immm$ to $I4/mmm$ structural transition would occur at 4 GPa accompanied by an $\sim 12\%$ volume collapse at the transition, when implementing the Perdew-Burke-Ernzerhof (PBE) + Hubbard

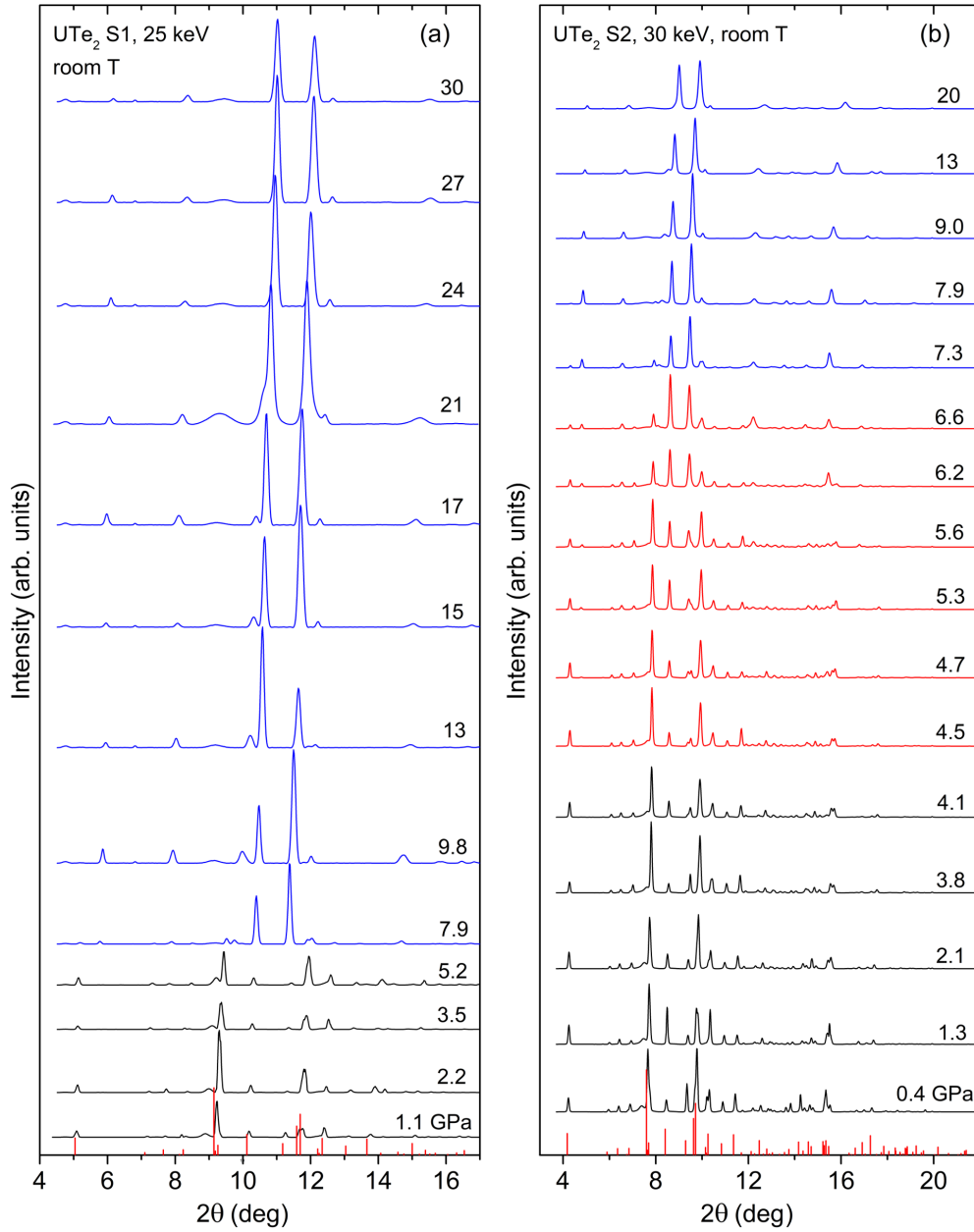


FIG. 1. XRD spectra of UTe_2 measured at various pressures between 0.4 and 30 GPa. (a) XRD patterns of UTe_2 from batch S1; (b) XRD spectra of UTe_2 from batch S2, which show a structural phase transition in progress between 5 and 7 GPa. The color scheme used to delineate the XRD spectra: Black: low- P phase; blue: high- P phase; and red: mixed low- P and high- P phases. Red vertical lines at the bottom of the figures indicate standard UTe_2 diffraction peaks based on Ref. [14].

U method with $U = 1$ or 2 eV [15]. This value is quite comparable to our experimental result of $\sim 10\%$ decrease in volume. The denser high-pressure $I4/mmm$ phase is achieved through a transition from a U-Te 8-coordinated distorted square

antiprism [9] to a 10-coordinated “bicapped cube,” in which lone-pair electrons of Te participate more in covalent bonding with U atoms, according to the calculation of the projected two-dimensional electron localization functions [15].

TABLE I. V_0 , K_0 , and dK_0/dP of UTe_2 in the orthorhombic and tetragonal phases at RT.

	Orthorhombic ($Immm$)			Tetragonal ($I4/mmm$)		
	V_0 (\AA^3)	K_0 (GPa)	dK_0/dP	V_0 (\AA^3)	K_0 (GPa)	dK_0/dP
UTe_2 S1	356.73	60 ± 5	6 ± 3	163.31	62 ± 13	3.6 ± 0.7
UTe_2 S2	356.63	57 ± 4	6.2 ± 2	160.31	67 ± 2	3.3 ± 0.4

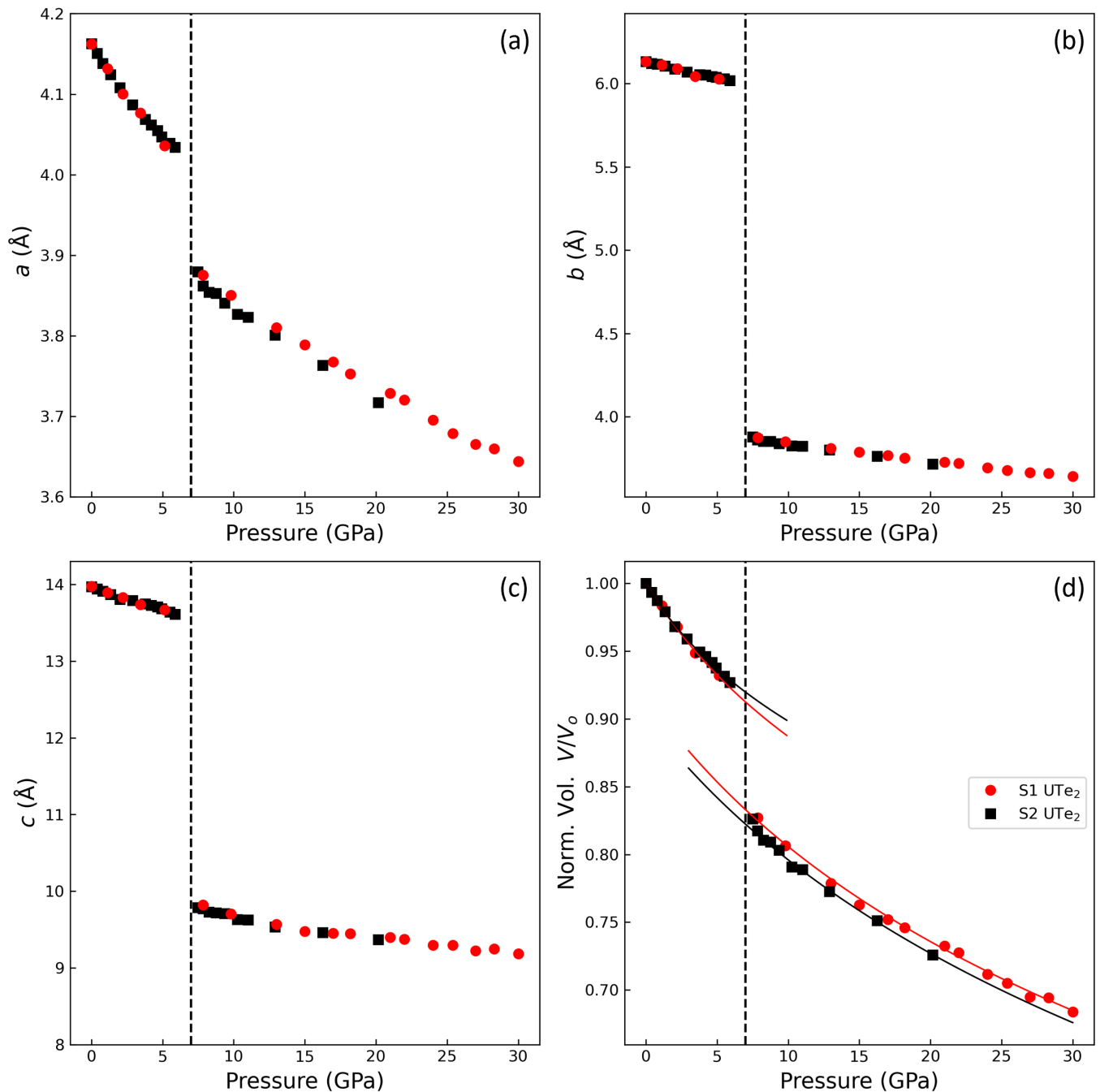


FIG. 2. Lattice parameters for two samples of UTe_2 vs pressure. (a)–(c) Lattice parameters a , b , and c . The current figure omits data points from the mixed phase for simplicity. (d): Normalized unit-cell volume (V/V_0) vs increasing pressure with respective third-order Birch-Murnaghan equation of state fits for both phases. The tetragonal phase V was multiplied by 2 and normalized to the $Immm$ V_0 to conserve the number of atoms across the structural phase transition.

Crystallographic and electronic structures are intimately interrelated, which underlines the importance of studying the pressure-induced structural phase transition in UTe_2 , since it can provide insights into how $5f$ electrons are involved in the bonding. When more $5f$ electrons participate in bonding in actinides it is typical to observe lower crystallographic symmetry [18,19]. With respect to the behavior of UTe_2 under pressure, $d_{\text{U-U}}$ in UTe_2 ($\sim 3.8 \text{ \AA}$) at ambient pressure is larger than the Hill limit ($\sim 3.5 \text{ \AA}$), a “rule-of-thumb” parameter representing the boundary between localization and

delocalization of $5f$ electrons for U compounds. Thus, we should expect magnetic order in UTe_2 instead of the superconductivity [20] observed in UTe_2 at ambient pressure. Strangely, the increase in $d_{\text{U-U}}$ at $\sim 5 \text{ GPa}$ indicates the $5f$ electrons of UTe_2 become more localized under pressure, which is consistent with the transition from the lower-symmetry orthorhombic phase to the higher-symmetry tetragonal phase, if the correspondence between $5f$ localization and higher crystal-structure symmetry is applicable to UTe_2 . The scenario of increased localization of $5f$ electrons

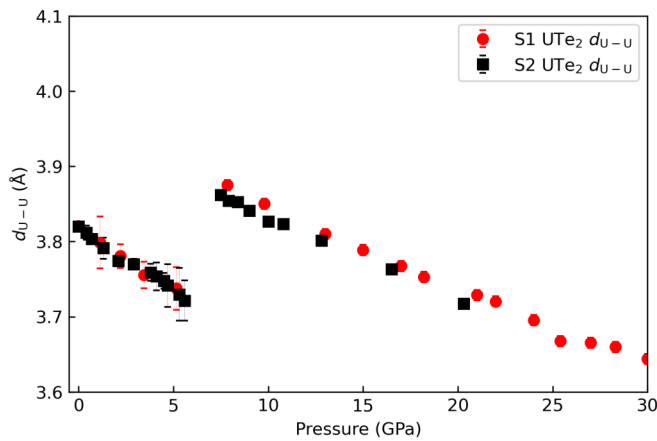


FIG. 3. The change in d_{U-U} in UTe_2 with pressure. For both samples, d_{U-U} increases at the structural phase transition from $Immm$ to $I4/mmm$ and steadily decreases with increasing pressure, where d_{U-U} in the high-pressure tetragonal phase at ~ 20 GPa equals the value in the lower-pressure orthorhombic phase at 6 GPa. The vertical bars represent the d_{U-U} measurement uncertainty. See Supplemental Material [13] for details.

in UTe_2 under pressure is supported by measurements of the electrical resistivity as a function of temperature reported in Ref. [10]. The measurements reveal the occurrence of superconductivity above 6 GPa with an upper critical field lower than the Pauli limit and Fermi-liquid behavior in the normal-state electrical resistivity $\rho(T)$ with a small coefficient (A) of the T^2 term, indicating that the electronic state of tetragonal UTe_2 is weakly correlated [10].

Huston *et al.* [9] pointed out that in other uranium chalcogenides such as USe and UTe , which have a ferromagnetic ground state and a value of d_{U-U} that exceeds the Hill limit, pressure also drives a transition from lower to higher structural symmetry [9,21]. It is interesting to note, regardless of whether the ground state is superconducting as in UTe_2 , or ferromagnetic as in USe and UTe , uranium chalcogenides seem inclined to transform into a higher-symmetry phase at high pressure. In the first-principles study of UTe_2 by Hu *et al.*, it was shown that covalent bonding between lone-pair electrons of Te and U atoms forms in the high-pressure tetragonal phase [15]. Perhaps this covalent bonding localizes $5f$ electrons, thus inducing the higher-symmetry tetragonal phase and increasing the bulk modulus appreciably since a three-dimensional network of covalent bonds (e.g., diamond and quartz) is usually quite rigid (although lattice stiffening is common in many kinds of pressure-induced phase changes) [22].

B. Probing $5f$ electrons by resonant x-ray emission spectroscopy

There have been several reports [5,11,23] of the electronic configuration of U in UTe_2 based on ambient or high-pressure studies using a variety of x-ray spectroscopy techniques. Among them, the integrated intensities of white lines at the $M_{4,5}$ ($M_4: d_{3/2} \rightarrow 5f_{5/2}$, $M_5: d_{5/2} \rightarrow 5f_{5/2,7/2}$) absorption edges were used to determine how the occupancy of $5f$ electrons varies with pressure [11]. RXES is an effective technique

that has been employed to investigate the role of $5f$ orbitals in the chemical bonding of U, Np, and Pu actinides [24]. Here, we explore the PFY-XAS of the L_3 absorption from $2p_{3/2}$ to unoccupied $6d$ and the RXES of the $L_{\alpha 1}$ emission from $3d_{5/2}$ to $2p_{3/2}$ to study the electronic state of UTe_2 . Though L_3 PFY-XAS and RXES spectroscopies are indirect ways to probe the $5f$ state, the higher incident and emission x-ray energies (~ 17 and ~ 13 keV, respectively) enable them to penetrate deeper inside materials to obtain information about the bulk [25,26]. The attenuation depth of x rays at 13.6 keV in UTe_2 ($\sim 15 \mu\text{m}$) is larger than our sample dimensions, which makes PFY-XAS and RXES measurements less sensitive to surface contamination [27]. Thanks to the line-narrowing effect due to the longer lifetime of $3d$ core hole than that of $2p$ core hole, we were able to see clear peak splitting in the RXES reflecting the multiconfigurations of $5f$ electrons in UTe_2 at ambient and high pressures.

Similar to their Ce and Yb compound cousins, the $5f^2$ ($J = 4$) and $5f^3$ ($J = 9/2$) configurations of U in many U intermetallics are not well separated in energy, leading to an intermediate (fluctuating) valence. Because different $5f$ -electron configurations are able to screen the $2p_{3/2}$ core hole differently, the $6d$ state will split in energy. More $5f$ electrons in a localized orbital means larger screening of the $2p$ core hole, so the Coulomb attraction between the core hole and the photoelectron is weakened, leading to a smaller energy separation between $2p$ and $6d$ [7]. The main consequence is the splitting of the white line in the PFY-XAS spectrum and of the emission peak in the RXES spectrum corresponding to the $2p \rightarrow 6d$ and $3d \rightarrow 2p$ transitions, respectively. This scenario applies well to Sm and Yb compounds [25,28,29], where both PFY-XAS and RXES measurements show the splitting features. However, it is usually not possible to observe the white-line or emission peak splitting in U compounds [26,30], although it has been possible to detect a shift in the white-line energy (e.g., UPd_2Al_3 [30] and $UCoGa_5$ [7]). Unlike $4f$ orbitals that are spatially confined to the vicinity of the lanthanide atomic cores, $5f$ orbitals are spatially more extended so they interact with conduction electrons or orbitals of neighboring atoms and contribute to metallic bonding and covalency. This delocalized character of the $5f$ electrons is reflected in the conduction band resulting in a narrower or flatter band and heavy-fermion properties in many U compounds. The change in screening strength due to a delocalized $5f$ orbital may not be strong enough to split the $6d$ states but may be able to shift the white line in PFY-XAS to higher energy [7,8]. Putting all of this together, extra caution is required when analyzing the pressure-induced changes in shape of the PFY-XAS and RXES spectra because they can originate from both valence changes and delocalization of $5f$ electrons.

C. High-pressure PFY-XAS

PFY-XAS measurements were taken by exciting the U L_3 -absorption edge with incident energy between 17.140 and 17.210 keV, while detecting emission at the U $L_{\alpha 1} = 13.614$ -keV line. Measurements were performed at RT at various pressures in diamond-anvil cells. As can be seen in Fig. 4, our PFY-XAS spectra for UTe_2 show the white line (main peak) from the $3d_{5/2}$ to $2p_{3/2}$ transition, a step-function-like

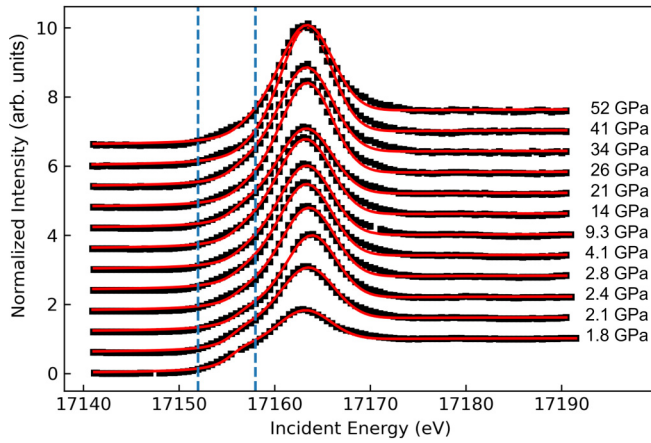


FIG. 4. PFY-XAS spectra of UTe_2 at different pressures. Curves are offset vertically for clarity. The emission intensity is normalized to the incident intensity. The two blue dashed lines enclose the region where the preedge quadrupole resonance occurs. The red curves are fits to the data, which are represented by solid black squares (see Supplemental Material [13] for more discussion).

background associated with the excitation into the continuum above the $6d$ states, and a small preedge shoulder at 6–7 eV below the white line. The shoulder can be attributed to a preedge quadrupole transition from $2p_{3/2}$ to $5f$ [31], which is usually smaller compared to the dipole-allowed white line. A similar feature on the left side of the white line was also found in U^{4+} , U^{5+} , and U^{6+} compounds, with a separation of 5–7 eV [26,31]. PFY-XAS spectra were normalized to the postedge step above 17.170 keV due to the excitation into the continuum using the open-sourced LARCH XAS analysis software [32], while additional post white-line flattening was applied to the data at $P = 1.8$ GPa due to synchrotron beam current instability that occurred during measurement (subsequent measurements did not have this issue). Spectra were fitted with a combination of an arctangent step function for data above 17.170 keV and a Gaussian function for the white-line, using the method outlined in Ref. [5]. The model was adjusted by varying all parameters with initial guesses for the step function width set to the uranium L_3 core-hole lifetime (~ 3.9 eV) and the step function position set by the first derivative of the interpolated PFY-XAS data curve. A detailed description and a figure showing all deconvoluted PFY-XAS spectra are presented in Supplemental Material [13].

Figure 5 shows the change in the white-line peak position under pressure, which was found by plotting the E_i of the peak maximum (see [Ref. [13]]). The white-line position blueshifts by ~ 0.7 eV up to 2.4 GPa. However, subsequent increases in pressure results in a redshift white line up to 4.1 GPa, after which there is little change in peak position up to 52 GPa. In previous studies of uranium intermetallics, changes in the U L_3 -edge white-line position were attributed to a change in U valence (or $5f$ -electron count) [5] or a change in the degree of delocalization of the $5f$ electrons [8]. Although there are contradictory conclusions on the $5f$ -electron count of UTe_2 (closer to 3 [11,33] vs closer to 2 [5]) at ambient pressure, UTe_2 is believed to have an intermediate valence.

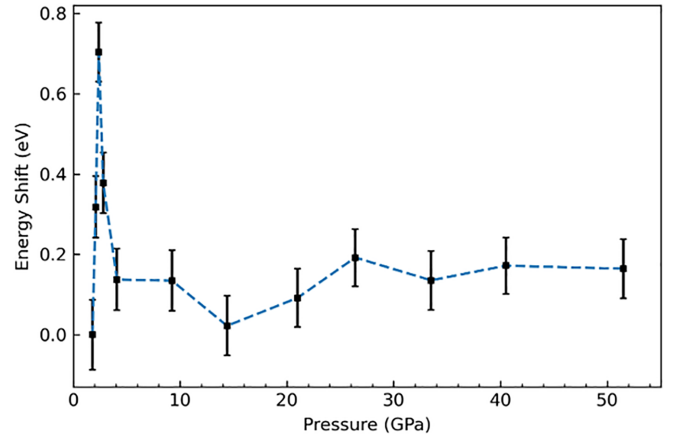


FIG. 5. Change in UTe_2 (batch S1) U L_3 -edge white-line position for UTe_2 with pressure relative to its position at 1.8 GPa. The vertical bars indicate the fitting error determined by estimated standard deviation [13].

Thomas *et al.* reported a small increase in U valence towards $4+$ above 1.25 GPa [5] in UTe_2 under pressure. Using U $M_{4,5}$ -edge XANES, Wilhelm *et al.* [11] observed an initial increase in valence towards $4+$ with pressure up to ~ 2 GPa, followed by a decrease in valence back to $3+$ with pressure. The white-line blueshift below 2.4 GPa can be ascribed to a pressure-induced delocalization of $5f$ electrons, or a transfer of spectral weight from $5f^3$ to $5f^2$ configuration, or a combination of both. Considering that $d_{\text{U-U}}$ is larger than the Hill limit, delocalization can occur through hybridization between the conduction band and $5f$ orbitals. Between 2.4 and 4.1 GPa, the observed redshift of the L_3 white line indicates a reverse trend: $5f$ electrons become more localized or there is an increase in the occupancy of the $5f^3$ configuration. The stable white-line position between 4.1 and 52 GPa reveals a $5f$ configuration with a stable degree of localization or a stable $5f$ configuration. The multiple origins of the white-line shift and the limited resolution of PFY-XAS data prevented an estimation of the $5f$ occupancy using standard first x-ray sum rules [34], so an estimation of the $5f$ occupancy was determined from deconvoluting RXES data instead, as described below.

D. High-pressure RXES

Representative RXES spectra of normalized L_{α_1} emission of UTe_2 at 2.1 GPa are shown in Fig. 6 as a function of incident x-ray energy (E_i) and transferred energy $E_t \equiv E_i - E_e$, where E_e is the emission energy. Even before deconvoluting configuration peaks there is a distinguishable doublet in the spectra at E_t below the white line. Peak positions stay nearly constant with E_t when E_i is lower than a threshold $E_T = 17.170$ keV, above which the nonresonant x-ray emission becomes dominant. This is characteristic of the resonant emission from $3d_{5/2}$ to $2p_{3/2}$ [6]. When E_i is higher than E_T , the excitation into the continuum overwhelms the excitation into the $6d$ states, and the emission spectra as a function of E_t shift linearly with E_i [6,7], as indicated by curves with $E_i > E_T$ in Fig. 6. The multiple peaks in the RXES emission spectra indicate multiconfigurational $5f$ states and agrees

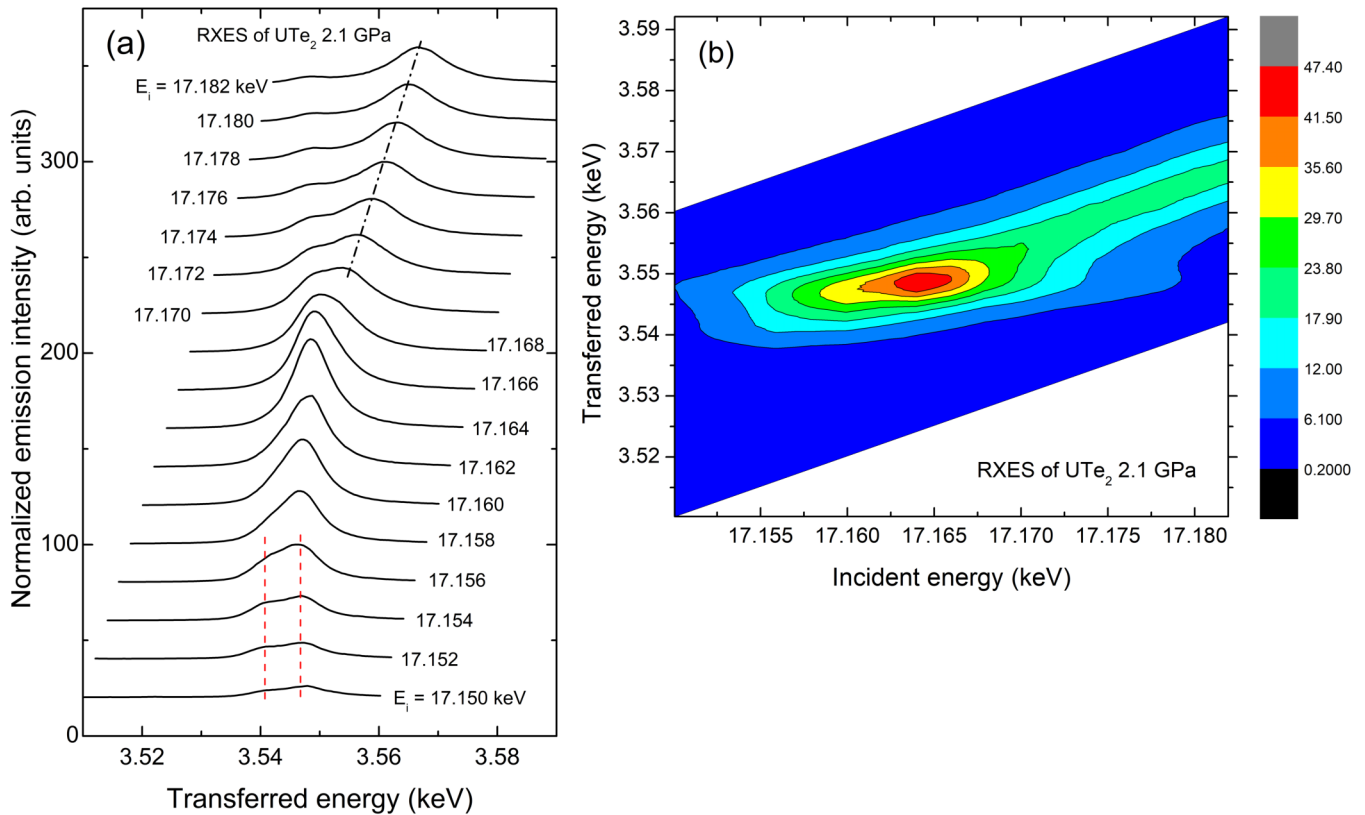


FIG. 6. RXES of UTe_2 (batch S1) at 2.1 GPa and RT. The red dashed lines indicate the two $5f$ configurations and the black dashed-dotted line indicates the shift in the nonresonant emission. The colors in the vertical scale bar of (b) show the normalized emission intensity. When $E_i \geq 17.170$ keV, a clear linear correlation can be seen between E_t at the emission maximum and E_i , indicating emission is from nonresonant excitation to the continuum.

with the PFY-XAS results. This suggests UTe_2 falls into a similar grouping of intermediate valence materials like SmB_6 [28], YbAl_3 [29], and UPd_2Al_3 [30].

The $5f$ -configuration weights ($5f^3$, $5f^2$) were calculated using the methodology in Ref. [7] for UCd_{11} and PuSb_2 . Since the total number of unoccupied $6d$ states is almost fixed, the relative excitation amplitude should be proportional to the occupancy in each $5f$ configuration [7]. The $5f$ -electron occupancy can then be calculated from the weighted sum of the integrated multiconfiguration peaks that are deconvoluted from the RXES spectra. Fortunately, unlike some other U intermetallics (e.g., UCd_{11} [7] and URu_2Si_2 [26]), our RXES data at energy below E_T clearly exhibit separate f^3 and f^2 peaks from the emission signal which helped identify the position of each configuration. Deconvolution of RXES data was accomplished via a nonlinear least-square-fitting PYTHON module (LMFIT) [35], by using two skewed Lorentzian functions corresponding to the f^3 and f^2 peaks, and a third skewed Lorentzian function corresponding to the fluorescence peak (FP) when E_i approached E_T of 17.170 keV to account for the electrons excited to the continuum.

An example multiconfiguration peak deconvolution at 2.4 GPa is shown in Fig. 7(a), where green and red peaks correspond to the $5f^3$ and $5f^2$ configurations, respectively, and the purple dashed FP corresponds to the nonresonant emission at selected E_i at 2.4 GPa. The areas under the curves are integrated to calculate the respective peak coefficients,

shown in Fig. 7(b). The resulting normalized peak coefficient data were then fitted to an associated Lorentzian (for $5f^3$ and $5f^2$ peaks) and integrated to calculate the configuration weight at each pressure. A more detailed summary for peak deconvolution and error analysis is discussed in Supplemental Material [13].

The $5f$ occupation (n_f) and f^3 and f^2 configuration fraction results are shown in Fig. 8. At low pressure, an initial $5f$ occupancy $n_f \sim 2.26$ (valence of 3.74) at 1.8 GPa decreases with pressure until a minimum at ~ 2.8 GPa where $n_f \sim 2.21$ (valence of 3.79). Afterwards, n_f increases with pressure until ~ 15 GPa where a plateau appears at $n_f \sim 2.24$ (valence of 3.76) and persists up to 52 GPa, indicating that the UTe_2 valence stays mostly constant at high pressures. The nonmonotonic valence change preceding the pressure-induced phase transition (5 GPa) qualitatively agrees with Ref. [11] which claims a valence maximum at about 2 GPa. The movement of the valence towards 3+ seems to be associated with the phase transition to the tetragonal structure, which has more room for U atoms due to the larger $d_{\text{U-U}}$ (see Fig. 3). The increased volume can more easily accommodate the U^{3+} ion, which has a larger ionic radius than the U^{4+} ion. Stability of the valence above 15 GPa appears to be consistent with PFY-XAS data, which exhibit little energy shift in the white-line position with pressure (see Fig. 5). Although the PFY-XAS white-line shift can be due to both the change in n_f and in the localization of $5f$ electrons [36], we do see some similarities

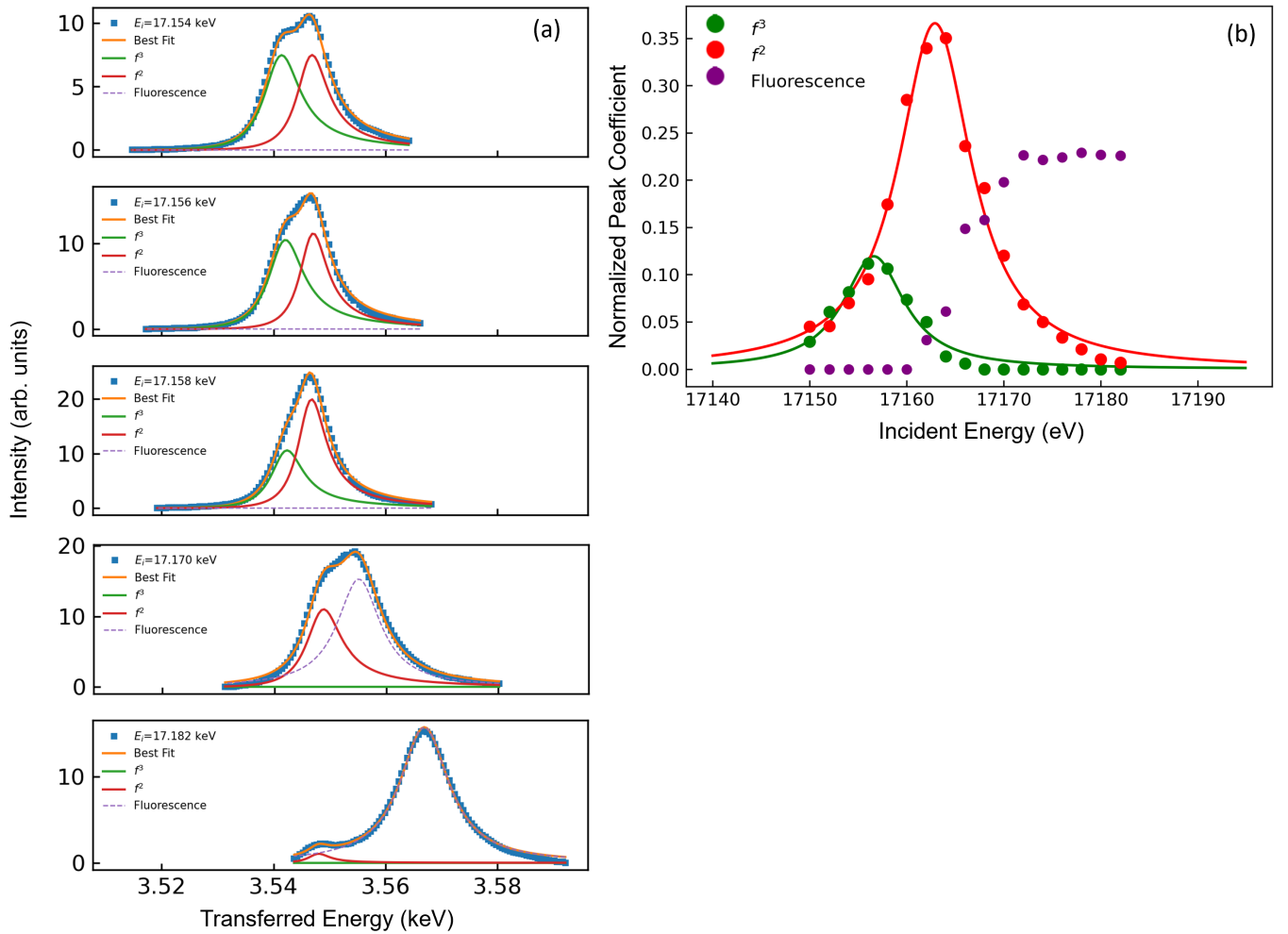


FIG. 7. (a) Multiconfiguration peak deconvolution for L_{α_1} RXES at 2.4 GPa, where green and red peaks correspond to the $5f^3$ and $5f^2$ peaks, respectively, and the purple dashed FP corresponds to the nonresonant emission. The FP dominates over $5f^3$ and $5f^2$ peaks when $E_i \geq 17170$ eV. (b) Normalized peak coefficient data plotted vs E_i . The fitted Lorentzians were integrated to calculate the configuration weights.

between the PFY-XAS and RXES data, as manifested in the mirrored curves in Figs. 5 and 8. The discrepancy between the two curves reflects the extra contribution to the PFY-XAS spectra from the change in the degree of itinerancy of $5f$ electrons under pressure.

A physical picture that has been applied to U-based heavy-fermion systems which provides insight into the transition from a nonmagnetic ground state to a magnetically ordered ground state in a Kondo lattice (KL) is provided by the “Doniach phase diagram” scenario [37]. This is based on an argument concerning the competition between two energy scales, the Kondo energy, which induces a demagnetization of the U ions, and the Ruderman-Kittel-Kasuya-Yosida (RKKY) interaction, which causes the localized magnetic moments on the U ions to form a magnetically ordered state. Both the Kondo effect and the RKKY interaction originate from an intra-atomic exchange interaction between the spins of the conduction electrons and the spins and orbital moments of localized f electrons.

For the Kondo effect to be operative, the intra-atomic exchange interaction between the conduction electron spins and U magnetic moments must be negative, i.e., favoring

their “antiferromagnetic” alignment. In a KL, this leads to the gradual formation of a coherent nonmagnetic ground state via compensation of the magnetic moments of the U ions by the spins of the conduction electrons. The characteristic temperature which describes the crossover to a nonmagnetic ground state is the Kondo temperature T_K . In the Doniach picture, the Kondo temperature is given by $T_K \sim T_F \exp[-1/N(E_F)|J_{\text{ex}}|]$, where T_F is the Fermi temperature and $N(E_F)$ is the density of states at the Fermi level E_F of the conduction electrons and J_{ex} is the strength of an onsite exchange interaction between the localized f moments and the conduction electrons. In contrast, the interatomic RKKY exchange interaction between localized magnetic moments, which is mediated by the spins of the conduction electrons, leads to magnetic ordering at a temperature T_{RKKY} (in the absence of the Kondo effect) that scales as J_{ex}^2 . In the Doniach scenario, the “knob” that tunes the ground state of the KL between a heavy Fermi liquid (HFL) and a magnetically ordered phase is the absolute value of the intra-atomic exchange-interaction parameter J_{ex} which is given by $J_{\text{ex}} = -V_{\text{kf}}^2/|\varepsilon_f|$, where V_{kf} represents the strength of the hybridization between localized f - and conduction-electron states and ε_f is the energy separating the localized

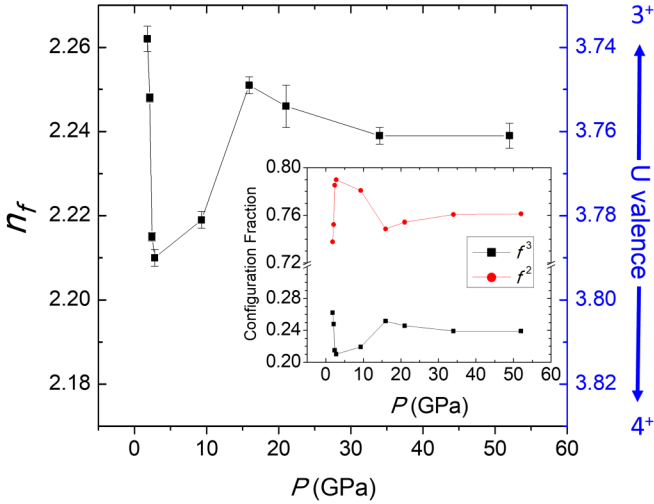


FIG. 8. The calculated $5f$ occupation n_f , and configuration fractions of f^3 and f^2 (inset) as a function of pressure for UTe_2 at RT. The vertical bars indicate the estimated standard deviation (refer to Supplemental Material [13]). The right y axis indicates the U valence, which is equal to the difference between the number of valence electrons of uranium atom (6) and the $5f$ occupancy.

f -electron state and the Fermi level E_F . This leads to the T vs $|J_{\text{ex}}|$ Doniach phase diagram in which the f -electron system exhibits magnetic order with an ordering temperature T_M vs $|J_{\text{ex}}|$ curve, with a dome shape that passes through a maximum with increasing $|J_{\text{ex}}|$ and then vanishes at a QCP when $|J_{\text{ex}}|$ reaches a critical value (i.e., when $T_{\text{RKKY}} = T_K$), at which point it enters a region with a nonmagnetic spin-compensated HFL ground state for larger values of $|J_{\text{ex}}|$.

The situation encountered in many heavy-electron systems studied under pressure involves the suppression of a magnetic phase, usually AFM, at a QCP at which the system undergoes a transition to a nonmagnetic HFL [38,39]. In the Doniach model, this transition corresponds to an increase of $|J_{\text{ex}}|$ with pressure. A dome-shaped region of unconventional superconductivity and/or V-shaped region of non-Fermi-liquid behavior [e.g., $\rho(T) \propto T$, $C(T)/T \propto -\ln(T)$] are frequently found in the vicinity of the QCP. In contrast, applying pressure to UTe_2 induces a transition from a nonmagnetic HFL, manifested at ambient pressure in a large Sommerfeld coefficient $\gamma = C(T)/T$ [1] and a large coefficient $A = \rho(T)/T^2$ [10], to an AFM state that appears between 1.5 and 4 GPa [5,10]. According to $\rho(T)$ and $ac-C(T)$ measurements under hydrostatic pressure by Thomas *et al.* [5], there is an AFM QCP at 1.3 GPa, estimated by extrapolating the boundaries of regions in T vs P , where the exponent n of the electrical resistivity $\rho(T) \propto T^n$ equals 1 near $T = 0$ K. Moreover, two superconducting phases are found at low pressure that appear to vanish at a pressure of ~ 1.6 GPa, where for one of the superconducting phases the T_c vs P data have a dome shape with a maximum in T_c near the AFM QCP. Knafo *et al.* [40] have recently reported similar behavior for the T_c vs P phase boundaries of the two superconducting phases and established that long-range incommensurate antiferromagnetic order occurs at 1.8 GPa by means of neutron-scattering measurements. The antiferromagnetic phase has a propagation vector close to that

of the wave vector where antiferromagnetic fluctuations were previously observed at ambient pressure [12,41–43]. Thus, in UTe_2 under pressure, two unconventional superconducting phases are apparently found near the AFM QCP at 1.3 GPa.

In the Doniach picture, the pressure-induced HFL–AFM transition found in UTe_2 implies a decrease in $|J_{\text{ex}}|$ with pressure. Since below 4 GPa $d_{\text{U-U}}$ decreases with pressure, we expect V_{kf} to be enhanced by pressure which, in turn, would imply that $|\epsilon_f|$ increases with pressure at a faster rate than V_{kf}^2 . This is similar to the scenario that was recently suggested for the relationship between the “hidden-order” (HO) phase and the AFM phase in the U-based HF compound, URu_2Si_2 [44,45]. In that case, application of pressure or generation of chemical pressure via substitution of the smaller Fe atom for Ru drives a transition from the nonmagnetic HO phase, which also hosts a coexisting unconventional superconducting phase, to an AFM phase, which implies a decrease in $|J_{\text{ex}}|$ within the context of the Doniach phase diagram [44,45].

Alternatively, the hybridization of the $5f$ and the itinerant conduction-band states, which determines J_{ex} and the Kondo screening, is governed by crystal structure and spin-orbit coupling. This sensitivity has led to the evolution of several pictures of U compounds with intermediate valence, involving orbitally selective hybridization. One such model, the so-called “dual-electron ansatz,” has been successfully applied to describe the physical properties of several uranium-based heavy-fermion compounds such as UPt_3 [46] and UPd_2Al_3 [47]. In the dual-electron model, it is assumed that two of the $5f$ electrons are localized and the remaining $5f$ electron is delocalized. The delocalized $5f$ states hybridize with conduction electron states and form conduction bands while the localized $5f$ electrons do not. The local exchange interaction between the two subsystems produces the mass enhancement of the delocalized quasiparticles. This approach accounts for measured de Haas–van Alphen frequencies of the heavy quasiparticles as well as their anisotropic heavy mass [46,47]. A similar dual model is the underscreened Anderson model, in which orbitally selective hybridization results in the formation of a hybridized itinerant $5f$ electron band and a set of unhybridized $5f$ bands. Like the underscreened Kondo model, the number of hybridization channels is insufficient to Kondo screen the $5f$ magnetic moments, allowing for long-range magnetic ordering of the partially screened moments. The underscreened Kondo and Anderson models have been applied to the uranium monochalcogenides [48,49]. More recently, an orbitally selective hybridization approach based on the k dependence of V_{kf} has been applied to UTe_2 [50].

It could be more than a coincidence that the U valence change towards $4+$, revealed in Ref. [5] and in our RXES data (from 1.8 to 2.8 GPa), is concurrent with the appearance of the AFM phase. In the dual models, a pressure-induced increase of the hybridization could produce a redistribution of the $5f$ electrons between the itinerant and localized states which, as suggested in Ref. [50], may result in the formation of an AFM phase due to a van Hove singularity. Above 5 GPa, according to our XRD results, $d_{\text{U-U}}$ increases abruptly due to the structural phase transition. This agrees with RXES results, which reveal a valence returning towards $3+$ just prior to the structural transition beginning at 5 GPa. The effect of the redistribution of $5f$ electrons between the hybridized and

unhybridized bands is manifested by the coherence temperature of the orthorhombic and tetragonal phases of UTe_2 . A shoulder is observed in the $\rho(T)$ curves at the coherence temperature T^* (~ 230 K) in the tetragonal phase [10], which is higher than the value of T^* (10–70 K [1,51]) in the orthorhombic phase. The anomalies in both the white-line position and n_f vs pressure curves lie well within the region of the AFM phase of UTe_2 , which appears to be sandwiched in between the low-pressure unconventional and high-pressure weakly correlated superconducting phases [10].

IV. CONCLUDING REMARKS

We studied the electronic and structural properties of UTe_2 under high pressure via RXES to 52 GPa and XRD to 30 GPa, pressures higher than those previously reported [5,10,11], and mapped the valence across the pressure-induced structural phase transition between 5 and 7 GPa from $Immm$ (orthorhombic) to $I4/mmm$ (body-centered tetragonal). Due to the higher-energy resolution of the RXES technique compared to traditional XANES, we were able to calculate the change of the U valence with pressure. The change from a lower- to a higher-symmetry crystal structure under high pressure, indicates that the $5f$ electrons become more localized and less itinerant in the high-pressure tetragonal phase [9], as one would expect from the viewpoint of a pressure-induced increase in d_{U-U} .

Over the whole pressure range investigated (1.8 to 30 GPa), d_{U-U} is larger than the Hill limit for U compounds, so magnetic ordering due to RKKY interactions could be anticipated. In reality, in this regime correlated electron phenomena such as unconventional superconductivity and heavy-fermion behavior often emerge. This implies that hybridization (V_{kf}) between localized $5f$ - and conduction-electron states and on-site Coulomb repulsion (U) between $5f$ electrons should play an important role in determining the electronic and magnetic properties of UTe_2 [9], like it does in other heavy-fermion systems, contributing to the limitations of the Hill limit in predicting the degree of $5f$ itinerancy in UTe_2 .

At RT, RXES data show UTe_2 has a valence of ~ 3.74 at 1.8 GPa, which changes to 3.79 at 2.8 GPa and then back to a value slightly smaller than it had at 1.8 GPa. Interestingly, the change in valence is accompanied by the structural phase transition at 5–7 GPa, suggesting a correlation between the U valence and crystal structure of UTe_2 . At pressures higher than 15 GPa, the U valence does not change with pressure. PFY-XAS data also revealed a nonmonotonic change

in the white-line position with pressure; however, due to complications associated with different mechanisms that lead to the shift in white-line position, it is difficult to reach a more definitive conclusion. It is worthwhile to point out that our PFY-XAS and RXES measurements were done at RT, whereas other results regarding the UTe_2 valence were based on spectroscopic measurements at low temperature in Ref. [33] (20 K), Ref. [5] (1.7 K), and Ref. [11] (2.7 K). It is known that for $4f$ systems with a small Kondo temperature, n_f depends strongly on temperature (e.g., YbAgCu_4 [52]). Our RXES results demonstrate well-separated resonant emissions from $5f^3$ and $5f^2$ configurations, which illustrate the advantage of using RXES in determining the UTe_2 valence. Extending RXES measurements to lower temperature, especially near the superconducting or magnetic ordering temperatures at high pressures, would reveal whether the U valence changes when UTe_2 undergoes these electronic and magnetic transitions.

ACKNOWLEDGMENTS

Research at the University of California (UC), San Diego was supported by the National Nuclear Security Administration (NNSA) under the Stewardship Science Academic Alliance Program through the US Department of Energy (DOE) under Grant No. DE-NA0004086, and the US DOE Basic Energy Sciences under Grant No. DE-FG02-04ER46105. This work was sponsored in part by the UC San Diego Materials Research Science and Engineering Center (UCSD MRSEC), supported by the National Science Foundation (NSF) under Grant No. DMR-2011924. Research at the University of Illinois Chicago was supported by the NNSA (Grant No. DE-NA-0003975, CDAC) and NSF (Grant No. DMR-2119308). Research at Florida State University and the National High Magnetic Field Laboratory was supported by NSF Cooperative Agreement No. DMR-2128556, and the DOE. Portions of this work were performed at HPCAT (Sector 16), Advanced Photon Source (APS), Argonne National Laboratory. HPCAT operations are supported by the DOE-NNSA Office of Experimental Sciences. The Advanced Photon Source is a US DOE Office of Science User Facility operated for the DOE Office of Science by Argonne National Laboratory under Contract No. DE-AC02-06CH11357. It is a pleasure to acknowledge informative discussions with Prof. A. Severing, Prof. L. H. Tjeng, A. Marino, and D. Christovam. We thank C. Kenney-Benson for assistance with x-ray measurements at HPCAT.

-
- [1] S. Ran, C. Eckberg, Q.-P. Ding, Y. Furukawa, T. Metz, S. R. Saha, I.-L. Liu, M. Zic, H. Kim, J. Paglione, and N. P. Butch, Nearly ferromagnetic spin-triplet superconductivity, *Science* **365**, 684 (2019).
- [2] D. Aoki, A. Nakamura, F. Honda, D. Li, Y. Homma, Y. Shimizu, Y. J. Sato, G. Knebel, J.-P. Brison, A. Pourret, D. Braithwaite, G. Lapertot, Q. Niu, M. Vališka, H. Harima, and J. Flouquet, Unconventional superconductivity in heavy fermion UTe_2 , *J. Phys. Soc. Jpn.* **88**, 043702 (2019).
- [3] S. Ran, I.-L. Liu, Y. S. Eo, D. J. Campbell, P. M. Neves, W. T. Fuhrman, S. R. Saha, C. Eckberg, H. Kim, D. Graf,

F. Balakirev, J. Singleton, J. Paglione, and N. P. Butch, Extreme magnetic field-boosted superconductivity, *Nat. Phys.* **15**, 1250 (2019).

- [4] G. Knebel, W. Knafo, A. Pourret, Q. Niu, M. Vališka, D. Braithwaite, G. Lapertot, M. Nardone, A. Zitouni, S. Mishra, I. Sheikin, G. Seyfarth, J.-P. Brison, D. Aoki, and J. Flouquet, Field-reentrant superconductivity close to a metamagnetic transition in the heavy-fermion superconductor UTe_2 , *J. Phys. Soc. Jpn.* **88**, 063707 (2019).

- [5] S. M. Thomas, F. B. Santos, M. H. Christensen, T. Asaba, F. Ronning, J. D. Thompson, E. D. Bauer, R. M. Fernandes,

- G. Fabbri, and P. F. S. Rosa, Evidence for a pressure-induced antiferromagnetic quantum critical point in intermediate-valence UTe_2 , *Sci. Adv.* **6**, eabc8709 (2020).
- [6] Y. Xiao, P. Chow, and G. Shen, High pressure X-ray emission spectroscopy at the advanced photon source, *High Press. Res.* **36**, 315 (2016).
- [7] C. H. Booth, Y. Jiang, D. L. Wang, J. N. Mitchell, P. H. Tobash, E. D. Bauer, M. A. Wall, P. G. Allen, D. Sokaras, D. Nordlund, T. -C. Weng, M. A. Torrez, and J. L. Sarrao, Multi-configurational nature of $5f$ orbitals in uranium and plutonium intermetallics, *Proc. Natl. Acad. Sci. USA* **109**, 10205 (2012).
- [8] F. Nasreen, D. Antonio, D. VanGennep, C. H. Booth, K. Kothapalli, E. D. Bauer, J. L. Sarrao, B. Lavina, V. Iota-Herbei, S. Sinogeikin, P. Chow, Y. Xiao, Y. Zhao, and A. L. Cornelius, High pressure effects on U L_3 x-ray absorption in partial fluorescence yield mode and single crystal x-ray diffraction in the heavy fermion compound UCd_{11} , *J. Phys.: Condens. Matter* **28**, 105601 (2016).
- [9] L. Q. Huston, D. Y. Popov, A. Weiland, M. M. Bordelon, P. F. S. Rosa, R. L. Rowland, B. L. Scott, G. Shen, C. Park, E. K. Moss, S. M. Thomas, J. D. Thompson, B. T. Sturtevant, and E. D. Bauer, Metastable phase of UTe_2 formed under high pressure above 5 GPa, *Phys. Rev. Mater.* **6**, 114801 (2022).
- [10] F. Honda, S. Kobayashi, N. Kawamura, S. Kawaguchi, T. Koizumi, Y. J. Sato, Y. Homma, N. Ishimatsu, J. Gouchi, Y. Uwatoko, H. Harima, J. Flouquet, and D. Aoki, Pressure-induced structural transition and new superconducting phase in UTe_2 , *J. Phys. Soc. Jpn.* **92**, 044702 (2023).
- [11] F. Wilhelm, J. P. Sanchez, D. Braithwaite, G. Knebel, G. Lapertot, and A. Rogalev, Investigating the electronic states of UTe_2 using X-ray spectroscopy, *Commun. Phys.* **6**, 96 (2023).
- [12] C. Duan, R. E. Baumbach, A. Podlesnyak, Y. Deng, C. Moir, A. J. Breindel, M. Brian Maple, E. M. Nica, Q. Si, and P. Dai, Resonance from antiferromagnetic spin fluctuations for superconductivity in UTe_2 , *Nature (London)* **600**, 636 (2021).
- [13] See Supplemental Material at <http://link.aps.org/supplemental/10.1103/PhysRevB.110.075140> for materials synthesis and characterization, high-pressure XRD experimental setup and analysis method, and high-pressure PFY-XAS and RXES experimental setups and analysis methods.
- [14] D. R. Boehme, M. C. Nichols, R. L. Snyder, and D. P. Matheis, An investigation of the tellurium-rich uranium tellurides using X-ray powder diffraction, *J. Alloys Compd.* **179**, 37 (1992).
- [15] K. Hu, Y. Zhao, Y. Geng, J. Yu, and Y. Gu, Pressure induced phase transition in heavy fermion metal UTe_2 : A first-principles study, *Phys. Lett. A* **451**, 128401 (2022).
- [16] B. H. Toby and R. B. Von Dreele, GSAS-II: The genesis of a modern open-source all-purpose crystallography software package, *J. Appl. Crystallogr.* **46**, 544 (2013).
- [17] K. Aoki, O. Shimomura, and S. Minomura, Crystal structure of the high-pressure phase of tellurium, *J. Phys. Soc. Jpn.* **48**, 551 (1980).
- [18] Y. K. Vohra and J. Akella, $5f$ bonding in thorium metal at extreme compressions: Phase transitions to 300 GPa, *Phys. Rev. Lett.* **67**, 3563 (1991).
- [19] K. T. Moore and G. van der Laan, Nature of the $5f$ states in actinide metals, *Rev. Mod. Phys.* **81**, 235 (2009).
- [20] H. H. Hill, in *Plutonium 1970 and Other Actinides*, edited by W. N. Miner (The Metallurgical Society of the AIME, New York, 1970).
- [21] N. Shekar, V. Kathirvel, B. Shukla, and P. Sahu, Phase transitions and structural stability of binary uranium intermetallics under high pressure: A Review, *Proc. Natl. Acad. Sci., India, Sect. A* **82**, 163 (2012).
- [22] N. W. Ashcroft and N. D. Mermin, *Solid State Physics* (Saunders College, Philadelphia, 1976), Chap. 19, p. 374.
- [23] S. Liu, Y. Xu, E. C. Kotta, L. Miao, S. Ran, J. Paglione, N. P. Butch, J. D. Denlinger, Y. -D. Chuang, and L. A. Wray, Identifying f -electron symmetries of UTe_2 with O-edge resonant inelastic x-ray scattering, *Phys. Rev. B* **106**, L241111 (2022).
- [24] T. Vitova, I. Pidchenko, D. Fellhauer, P. S. Bagus, Y. Joly, T. Pruessman, S. Bahl, E. Gonzalez-Robles, J. Rothe, M. Altmair, M. A. Denecke, and H. Geckeis, The role of the $5f$ valence orbitals of early actinides in chemical bonding, *Nat. Commun.* **8**, 16053 (2017).
- [25] C. Dallera, E. Annese, J.-P. Rueff, A. Palenzona, G. Vankó, L. Braicovich, A. Shukla, and M. Grioni, Determination of pressure-induced valence changes in $YbAl_2$ by resonant inelastic x-ray emission, *Phys. Rev. B* **68**, 245114 (2003).
- [26] C. H. Booth, S. A. Medling, J. G. Tobin, R. E. Baumbach, E. D. Bauer, D. Sokaras, D. Nordlund, and T.-C. Weng, Probing $5f$ -state configurations in URu_2Si_2 with U L_{III} -edge resonant x-ray emission spectroscopy, *Phys. Rev. B* **94**, 045121 (2016).
- [27] B. L. Henke, E. M. Gullikson, and J. C. Davis, X-ray interactions: Photoabsorption, scattering, transmission, and reflection at $E = 50-30000$ eV, $Z = 1-92$, *At. Data Nucl. Data Tables* **54**, 181 (1993).
- [28] N. P. Butch, J. Paglione, P. Chow, Y. Xiao, C. A. Marianetti, C. H. Booth, and J. R. Jeffries, Pressure-resistant intermediate valence in the Kondo insulator SbB_6 , *Phys. Rev. Lett.* **116**, 156401 (2016).
- [29] R. S. Kumar, A. Svane, G. Vaitheeswaran, V. Kanchana, E. D. Bauer, M. Hu, M. F. Nicol, and A. L. Cornelius, Pressure-induced valence change in $YbAl_3$: A combined high-pressure inelastic x-ray scattering and theoretical investigation, *Phys. Rev. B* **78**, 075117 (2008).
- [30] J.-P. Rueff, S. Raymond, A. Yaresko, D. Braithwaite, P. Leininger, G. Vankó, A. Huxley, J. Rebizant, and N. Sato, Pressure-induced f -electron delocalization in the U-based strongly correlated compounds UPd_3 and UPd_2Al_3 : Resonant inelastic x-ray scattering and first-principles calculations, *Phys. Rev. B* **76**, 085113 (2007).
- [31] T. Vitova, K. O. Kvashnina, G. Nocton, G. Sukharina, M. A. Denecke, S. M. Butorin, M. Mazzanti, R. Caciuffo, A. Soldatov, T. Behrends, and H. Geckeis, High energy resolution x-ray absorption spectroscopy study of uranium in varying valence states, *Phys. Rev. B* **82**, 235118 (2010).
- [32] M. Newville, Larch: An analysis package for XAFS and related spectroscopies, *J. Phys. Conf. Ser.* **430**, 012007 (2013).
- [33] S. I. Fujimori, I. Kawasaki, Y. Takeda, H. Yamagami, A. Nakamura, Y. Homma, and D. Aoki, Core-level photoelectron spectroscopy study of UTe_2 , *J. Phys. Soc. Jpn.* **90**, 015002 (2021).
- [34] A. F. Starace, Potential-barrier effects in photoabsorption. I. General theory, *Phys. Rev. B* **5**, 1773 (1972).
- [35] M. Newville, T. Stensitzki, D. B. Allen, and A. Ingargiola, LMFIT: Non-linear least-square minimization and curve-fitting for Python, Zenodo (2014), doi:10.5281/zenodo.11813.
- [36] C. H. Booth, S. A. Medling, Y. Jiang, E. D. Bauer, P. H. Tobash, J. N. Mitchell, D. K. Veirs, M. A. Wall, P. G. Allen, J. J. Kas,

- D. Sokaras, D. Nordlund, and T. -C. Weng, Delocalization and occupancy effects of $5f$ orbitals in plutonium intermetallics using L_3 -edge resonant x-ray emission spectroscopy, *J. Electron Spectrosc. Relat. Phenom.* **194**, 57 (2014).
- [37] S. Doniach, The Kondo lattice and weak antiferromagnetism, *Physica B+C* **91**, 231 (1977).
- [38] B. D. White, J. D. Thompson, and M. B. Maple, Unconventional superconductivity in heavy-fermion compounds, *Physica C (Amsterdam, Neth.)* **514**, 246 (2015).
- [39] C. D. O'Neill, J. L. Schmeh, and A. D. Huxley, Multicomponent odd-parity superconductivity in UAu_2 at high pressure, *Proc. Natl. Acad. Sci. USA* **119**, e2210235119 (2022).
- [40] W. Knafo, T. Thebault, P. Manuel, D. D. Khalyavin, F. Orlandi, E. Ressouche, K. Beauvois, G. Lapertot, K. Kaneko, D. Aoki, D. Braithwaite, G. Knebel, and S. Raymond, Incommensurate antiferromagnetism in UTe_2 under pressure, [arXiv:2311.05455](https://arxiv.org/abs/2311.05455).
- [41] C. Duan, K. Sasmal, M. B. Maple, A. Podlesnyak, J.-X. Zhu, Q. Si, and P. Dai, Incommensurate spin fluctuations in the spin-triplet superconductor candidate UTe_2 , *Phys. Rev. Lett.* **125**, 237003 (2020).
- [42] W. Knafo, G. Knebel, P. Steffens, K. Kaneko, A. Rosuel, J.-P. Brison, J. Flouquet, D. Aoki, G. Lapertot, and S. Raymond, Low-dimensional antiferromagnetic fluctuations in the heavy-fermion paramagnetic ladder UTe_2 , *Phys. Rev. B* **104**, L100409 (2021).
- [43] N. P. Butch, S. Ran, S. R. Saha, P. M. Neves, M. P. Zic, J. Paglione, S. Gladchenko, Q. Ye, and J. A. Rodriguez-Rivera, Symmetry of magnetic correlations in spin-triplet superconductor UTe_2 , *npj Quantum Mater.* **7**, 39 (2022).
- [44] A. Amorese, M. Sundermann, B. Leedahl, A. Marino, D. Takegami, H. Gretarsson, A. Gloskovskii, C. Schlueter, M. W. Haverkort, Y. Huang, M. Szlowska, D. Kaczorowski, S. Rang, M. B. Maple, E. D. Bauer, A. Leithe-Jasper, P. Hansmann, P. Thalmeier, L. H. Tjeng, and A. Severing, From antiferromagnetic and hidden order to Pauli paramagnetism in UM_2Si_2 compounds with $5f$ electron duality, *Proc. Natl. Acad. Sci. USA* **117**, 30220 (2020).
- [45] A. Marino, D. S. Christovam, C. F. Chang, J. Falke, C. Y. Kuo, C. N. Wu, M. Sundermann, A. Amorese, H. Gretarsson, E. Lee-Wong, C. M. Moir, Y. Deng, M. B. Maple, P. Thalmeier, L. H. Tjeng, and A. Severing, Fe substitution in URu_2Si_2 : Singlet magnetism in an extended Doniach phase diagram, *Phys. Rev. B* **108**, 085128 (2023).
- [46] G. Zwicknagl, A. N. Yaresko, and P. Fulde, Microscopic description of origin of heavy quasiparticles in UPt_3 , *Phys. Rev. B* **65**, 081103(R) (2002).
- [47] P. Thalmeier, Dual model for magnetic excitations and superconductivity in UPd_2Al_3 , *Eur. Phys. J. B* **27**, 29 (2002).
- [48] N. B. Perkins, M. Nunez-Regueiro, B. Coqblin, and J. R. Iglesias, Under-screened Kondo lattice model applied to heavy fermion uranium compounds, *Phys. Rev. B* **76**, 125101 (2007).
- [49] C. Thomas, A. S. D. Simoes, J. R. Iglesias, C. LaCroix, N. B. Perkins, and B. Coqblin, Application of the $S = 1$ under-screened Anderson lattice model to Kondo uranium and neptunium compounds, *Phys. Rev. B* **83**, 014415 (2011).
- [50] B. Kang, Y. Lee, L. Ke, H. Kim, M.-H. Kim, and C. H. Park, Dual nature of magnetism driven by momentum dependent f - d Kondo hybridization, *Commun. Phys.* **7**, 186 (2024).
- [51] Y. S. Eo, S. Liu, S. R. Saha, H. Kim, S. Ran, J. A. Horn, H. Hodovanets, J. Collini, T. Metz, W. T. Fuhrman, A. H. Nevdomskyy, J. D. Denlinger, N. P. Butch, M. S. Fuhrer, L. A. Wray, and J. Paglione, c -axis transport in UTe_2 : Evidence of three-dimensional conductivity component, *Phys. Rev. B* **106**, L060505 (2022).
- [52] C. Dallera, M. Grioni, A. Shukla, G. Vankó, J. L. Sarrao, J.-P. Rueff, and D. L. Cox, New spectroscopy solves an old puzzle: The Kondo scale in heavy fermions, *Phys. Rev. Lett.* **88**, 196403 (2002).